94 Journal of Electrical Engineering & Technology Vol. 6, No. 1, pp. 94~103, 2011
DOI: 10.5370/JEET.2011.6.1.094

Design and Analysis of Hybrid Stator Bearingless SRM

Dong-Hee Lee* and Jin-Woo Ahn†

Abstract – This paper presents a novel bearingless switched reluctance motor (BLSRM) with decoupled torque and suspending stator poles. BLSRM is different from conventional bearingless switched reluctance motors (SRMs) because its suspending poles are separated from the torque poles. Perpendicularly placed suspending poles are designed to produce a continuous radial force to suspend the rotor. Due to the independent suspending and torque poles, BLSRM produces a suspending force with excellent linearity according to the rotor position and independent characteristics of the torque current. The air-gap is easier to control than in conventional SRMs with their linear and independent characteristics. Furthermore, to verify the proposed structure, a mathematical model for the suspending force is derived. Finite element analysis is also employed to compare BLSRM and conventional SRMs expressions of suspending force. A prototype motoris designed and manufactured to verify the effectiveness of the proposed bearingless structure.

Keywords: SRM, Bearingless structure, Hybrid stator, FEM analysis, Suspending force, Separated poles

1. Introduction

Switched reluctance motors (SRMs) performance excellently in special environments because of their inherent fault tolerance, robustness, tolerance to high temperatures, and intense temperature variations [1].

SRMs have the advantage of being bearingless motors due to the inherent radial magnetic attraction force between the rotor and stator poles. This radial force can suspend the rotor. As a result, the mechanical bearings that are placed in the front and end parts of the motors can be replaced with a suitable inherent radial force. A bearingless structure is very useful for mechanical maintenance, given that it reduces both friction and temperature and increases environmental fault tolerance. Since the bearing-like ability and the motor are integrated into a compact unit, and bearingless motors are essentially maintenance-free, they are particularly suitable for operating in special environments, such as blood pumps [2]-[4].

Recently, several structures of bearingless switched reluctance motors (BLSRM) have been proposed. A radial force and torque control scheme has been proposed for the bearingless control of a 12/8 pole SRM, which has auxiliary windings for radial force at the stator poles [4]-[5].

The auxiliary winding produces a radial force for rotor levitation between the stator and rotor poles. Magnetic saturation has been considered in the force control algorithm, and thus, stable operation can be achieved. In the other report [6], a method for a BLSRM with 8/6 type has been proposed. In this method, three windings are loaded with different currents in each commutating period. Three torques and three lateral forces can be generated. One hybrid rotor structure, referred to as a Morrison rotor, has also been introduced [7]. The rotor is a hybrid composed of a circular lamination stack used to improve levitation performance, as well as a multi-pole lamination stack from a conventional rotor.

This paper presents a novel BLSRM with separated torque and suspending stator poles. Although two types of windings are placed on the stator poles, each only contains one winding. The proposed separated poles can reduce magnetic coupling between the radial force and the torque from each winding as opposed to double-winding types. It can also maintain good mechanical stiffness compared with SRMs having similar axial length. Since the separated windings produce related torque or radial force with negligible magnetic coupling, BLSRMs exhibit excellent independent characteristics between torque and suspending force. In addition, the produced suspending force displays excellent linearity according to the position of the rotors. As a result, air-gap control in BLSRMs is easier to accomplish compared with conventional SRMs.

This paper discusses the design and analyzes the prototype motor and its characteristics. Experimental results and comparison with corresponding simulations are provided.

1.1 Conventional BLSRM

Fig. 1 shows the typical structures of a conventional BLSRM. Even if the winding configurations on the stator pole of both structures differ, their main bodies are still based on a standard SRM. Torque and radial force are the function of current and rotor position, respectively. The effective torque region is within the ascending region of

† Corresponding Author: Dept. of Mechatronics Engineering, Kyungsung University, Korea. (jwahn@ks.ac.kr)
* Dept. of Mechatronics Engineering, Kyungsung University, Korea.
Received: June 3, 2010; Accepted: July 30, 2010

inductance, whereas effective radial force only occurs close to the aligned position.

Fig. 2 shows the inductance, radial force, and torque for a standard BLSRM structure. The effective torque region is from θ_1 to θ_3. The available radial force region is from θ_2 to θ_4. The overlap region between torque and radial force is from θ_2 to θ_3. Ideally, a motor should operate in this overlap region, as shown in the hatched part, in which enough torque and radial force can be generated simultaneously.

However, because of the inherent principle of torque and radial force in conventional SRMs, this overlap region is very narrow. An operating point has to be selected, which results in a compromise between torque and radial force in conventional structures. Accordingly, regions for torque and radial force cannot be utilized fully. Therefore, current has to be increased and dwell angle should be moved toward an aligned position to gain enough radial force. This means that both torque and radial force increase at the expense of larger current value, which then results in higher copper loss and thermal problems. On the other hand, torque and radial force are generated simultaneously by the same winding current. They correspond to the nonlinear functions of current and position. It is difficult to decouple torque from radial force. All previous BLSRMs are based on a general SRM structure that manifests the abovementioned problems.

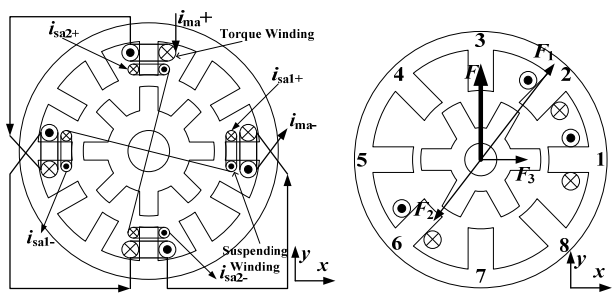

(a) Differential winding (b) Single winding

Fig. 1. Typical BLSRM.

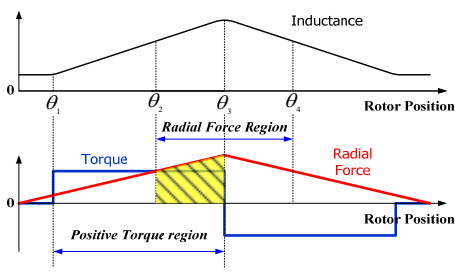

Fig. 2. Inductance, torque, and radial force of conventional SRM.

1.2 Proposed BLSRM

Fig. 3 shows the proposed novel 8/10 BLSRM with separated torque and radial force winding. This BLSRM is different from conventional structures because two types of stator poles are included on the stator. One is a torque pole

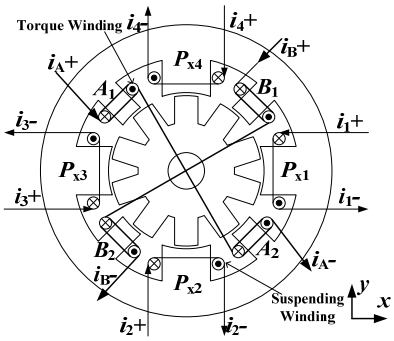

(a) Structure and windings

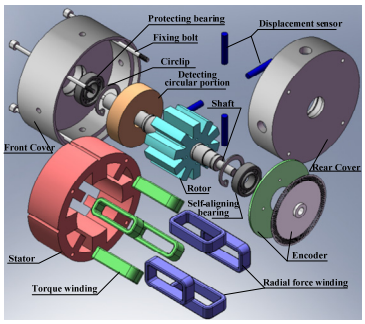

(b) Configuration of proposed motor

Fig. 3. Proposed BLSRM.

(i.e., A_1, A_2, B_1, and B_2), which mainly produces rotational torque. The other is radial force pole (i.e., P_{x1}, P_{x2}, P_{x3}, and P_{x4}), which mainly generates a radial force to suspend the rotor and shaft. In determining continuous radial force, the selected pole arc of the radial force is should not be less than one pole pitch of the rotor. Windings on poles A_1 and A_2 are connected in a series for torque winding A, whereas windings on poles B_1 and B_2 are connected in a series for torque winding B. Windings on poles P_{x1}, P_{x2}, P_{x3}, and P_{x4} are independently controlled to construct four radial forces in the x- and y-directions. Fig. 3(b) shows the configuration of the proposed structure.

Compared with conventional BLSRMs, the main features of the proposed structure include the following:

A. Separate Single Winding

Only one winding is intertwined on each stator pole. Thus, it is easier to manufacture compared with conventional structures. Separated winding also develops a separate torque or radial force that is different from the general single-winding type.

B. Wide Radial Force Region

Since the pole arc of the radial force is not less than one rotor pole pitch, the overlap area between radial force and rotor poles is constant at any rotor position. When the air gap length, current, and winding turns are fixed, radial force would be the only factor related to the overlap area. Therefore, a wide and almost constant radial force can be achieved at a given current. Compared with conventional types, the available radial force region is larger.

C. Natural Decoupling Characteristics of Torque from Radial Force

Given the constant overlap area between radial force and rotor poles, the inductance variations for the torque winding with respect to rotor position is small with fixed excitation current. Consequently, the torque produced by radial force winding is small. Radial force control has almost no influence on torque control for any arbitrary rotor position. Thus, decoupling control between torque and force can be realized naturally.

D. Simple Control Algorithm

Based on the abovementioned advantages, a simple algorithm is applied to implement the steady suspension of the rotor and shaft.

However, in the proposed structure, half of the stator poles are used for the torque. Unlike in conventional 8/10 SRM structures, power density is halved. Meanwhile, in other conventional BLSRMs, negative torque is unavoidable while performing suspending control. Thus, power density is reduced in a bearingless motor structure. Compared with magnetic bearings, bearingless motors show obvious advantages, such as compact structures.

1.3 Radial Force Calculation

Fig. 4 shows the magnetic flux distribution and flux path of the suspending stator and the rotor pole according to rotor position. In Fig. 4, β_r is the rotor pole arc, τ_r denotes the rotor pole pitch, B_{ss} is the pole arc of the suspending stator pole, and β_0 is defined as half of τ_r-β_r. The air gap of the stator and rotor poles is defined as l_a. Assuming that r is the rotor radius, subscripts x and y are the moving distances in the x- and y-directions, respectively.

In Fig. 4(a), the suspending stator pole is aligned as one rotor pole; in Fig. 4(b), it is aligned as two rotor poles. The suspending pole arc, β_{ss}, is designed as τ_r (rotor pole pitch). Therefore, the suspending pole is always aligned by one rotor pole arc β_r to produce a constant radial force.

During calculation, the saturation and leakage flux of the magnetic circuit in the suspending pole are neglected. Axial eccentricity is small compared with the length of the air-gap displacement.

The permeance of P_{x1} pole can be calculated in the case of Fig. 4(a) as follows:

$$P_{x1}=\frac{\mu_0 l\beta_r}{l_0-x+\frac{y\theta}{2}}+3\frac{\mu_0 l}{a\pi-2}\left[a\cdot\ln\frac{al_a+\beta_0}{al_a}+\frac{a\pi-4}{\pi}\cdot\ln\frac{2l_a+\pi\beta_0}{2l_a}\right]-\frac{\mu_0 l}{a\pi-2}\left[a\cdot\ln\frac{al_a-r\theta-y-\beta_0}{al_a}+\frac{a\pi-4}{\pi}\cdot\ln\frac{2l_a+\pi(-r\theta-y+\beta_0)}{2l_a}\right] \quad (1)$$

In the case of Fig. 4(b), it can be derived as follows:

$$P_{x1}=\frac{\mu_0 l\beta_r}{l_0-x+\frac{y\theta}{2}}+3\frac{\mu_0 l}{a\pi-2}\left[a\cdot\ln\frac{al_a+\beta_0}{al_a}+\frac{a\pi-4}{\pi}\cdot\ln\frac{2l_a+\pi\beta_0}{2l_a}\right]-\frac{\mu_0 l}{a\pi-2}\left[a\cdot\ln\frac{al_a+r\theta+y-\beta_0}{al_a}+\frac{a\pi-4}{\pi}\cdot\ln\frac{2l_a+\pi(r\theta+y-\beta_0)}{2l_a}\right] \quad (2)$$

where l is the axial length of the stator and the rotor core; μ_0 denotes free-permeability; and a is the coefficient for FEM analysis. The suspending radial force at P_{x1} winding stator pole can be derived from permeance as follows:

$$F_x=\frac{\partial W_{x1}}{\partial x}=\frac{1}{2}\cdot\frac{\partial P_{x1}}{\partial x}\left(N_{x1}\cdot i_{x1}\right)^2 \quad (3)$$

$$F_y=\frac{\partial W_{x1}}{\partial y}=\frac{1}{2}\cdot\frac{\partial P_{x1}}{\partial y}\left(N_{x1}\cdot i_{x1}\right)^2 \quad (4)$$

where N_{x1} and i_{x1} are the turn numbers of the suspending winding of P_{x1} pole and winding current, respectively.

Fig. 5 shows the comparative results between FEA and the calculation model. The values obtained from calculation based on the permeance model coincide well with FEA results.

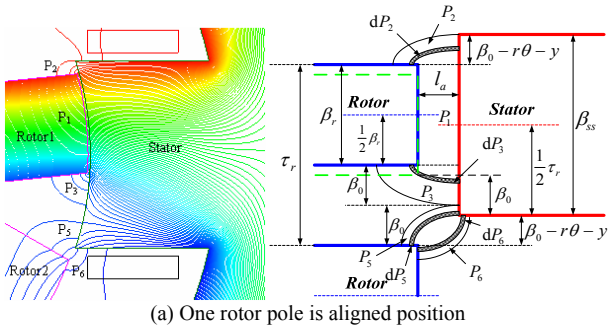

(a) One rotor pole is aligned position

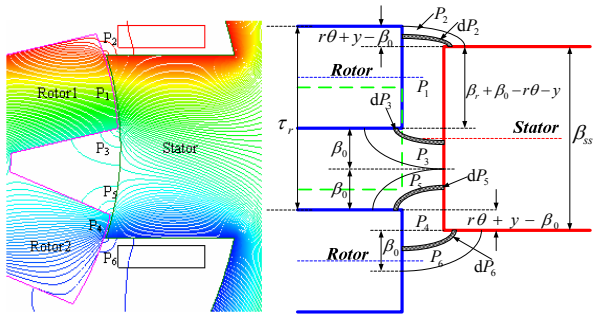

(b) Two rotor poles are aligned

Fig. 4. Simplified equivalent magnetic circuit of the air-gap.

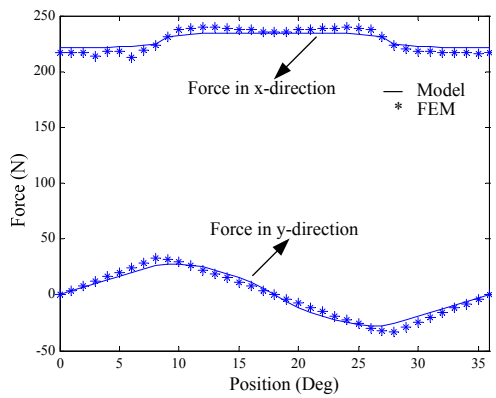

Fig. 5. Comparative results between the permeance model and FEM.

2. Design of the Proposed BLSRM

Due to its application field, radial force requires more attention compared with the torque in BLSRM. This section presents the design principle for the proposed BLSRM structure.

2.1 Selection of Pole Number

For the proposed structure, radial forces from stator poles are essential utilized by suspending force. Considering symmetry of structure and output torque, the number of torque poles should not be less than four. Therefore, the sum of stator poles should be at least eight.

As for the selection of rotor pole number, it is restricted by following conditions : A. The pole number for the rotor should be even. Two stator poles in the diameter direction should belong to the same phase. This requires the corresponding rotor poles to exhibit the same relative positions as the stator poles.

B. Rotor poles should match the number of stator poles. This requires the SRM to provide a continuous output torque. The general combination of pole numbers for stators and rotors is shown in Table 1 [5].

In Table 1, q is the phase number, while N_s and N_r are the pole number of the stator and rotor, respectively.

The relationship between switching frequency and rotating speed is shown in (5):

$$f = qN_r n / 60 \tag{5}$$

In (5), f is the switching frequency and n is the rotor speed in rpm. Switching frequency increases with phase number, rotor pole number, and speed. The phase and pole number of the rotor should be reduced in order to minimize switching and core losses in the stator. When the pole number of the stator is 8, the pole number of the rotor is 6 or 10.

Based on the proposed structure shown in Fig. 6, the pole arc of radial force β_{ss} and rotor pole pitch τ_r is equal to

Table 1. General combination of pole numbers

Q	N_s	N_r	
3	6	4	8
4	8	6	10
5	10	8	12

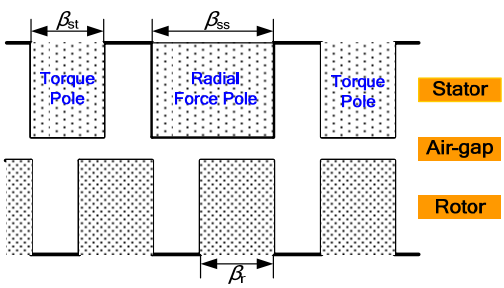

Fig. 6. Simplified structure of proposed BLSRM.

$$\beta_{ss} \geq \tau_r = 360^\circ / N_r \tag{6}$$

A higher N_r, leads the remaining space for installing the torque pole to be smaller. Thus, the number of rotor poles is fixed to 10.

2.2 Selection of Pole Arc

The pole arc selection is different from previous BLSRM structures. Three main parameters are characterized, as shown in Fig. 6: torque pole arc β_{st}, radial force pole arc βss, and rotor pole arc β_r. To obtain the largest possible variation in phase inductance with respect to rotor position, the interpolar arc of the rotor must exceed torque pole arc. This leads to the condition [6]

$$\beta_r + \beta_{st} \leq \frac{360^\circ}{N_r} \tag{7}$$

ensuring that no overlapping occurs when the rotor is in an unaligned position relative to the torque poles of one phase. Therefore, very low inductance can be obtained. A further constraint on pole arcs is that the torque pole arc is often made slightly smaller than the rotor pole arc. This gives the condition,

$$\beta_{st} \leq \beta_r \tag{8}$$

causing a slight increase in the slot area. To produce unidirectional torque in 360°, the torque pole arc should not be smaller than the step angle; otherwise, there will be "dead points," in which no torque is generated.

$$\beta_{st} \geq \frac{360^\circ}{qN_r} \tag{9}$$

which is incompatible with (8). However, to ensure that there is space for the winding, another constraint should be given:

$$\frac{1}{2}(\beta_{ss} + \beta_{st}) < \frac{360^\circ}{N_s} \tag{10}$$

The pole arc constraints for the design of parameters from (6)-(10) can be graphically described by a solid-line shaped tetrahedron, as shown in Fig. 7, where the performance of the proposed structure can be determined according to the points located on the geometric graph.

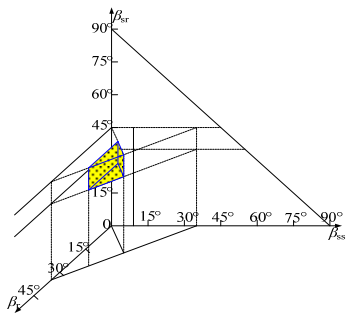

Fig. 7. Pole-arc constraints of the proposed SRM.

2.3 Selection of Air Gap Length

Torque is inversely proportional to air-gap length while radial force is inversely proportional to the square of air-gap length. Thus, any decrease in air-gap results in an increase in electromagnetic torque and radial force. The reason for this is that aligned inductance is very sensitive to air-gap length; however, in the case of unaligned inductance, it is the opposite. Aligned inductance increases with a decrease in air-gap length. Unaligned inductance can be kept at an almost constant value. The above analysis is shown in Fig. 8. However, the manufacturing tolerance supported in the production environment is an important factor driving minimum air-gap length determination. Therefore, air-gap length is selected at the range of 0.25 to 0.5 mm.

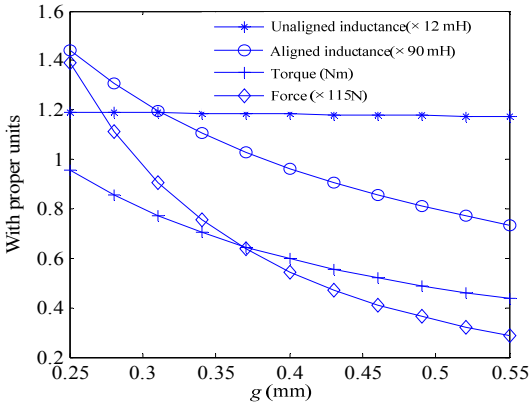

Fig. 8. Effects of air gap length on inductances, torque, and force.

3. Analysis of the Proposed BLSRM

3.1 Characteristics of the Proposed SRM in Normal Condition

Torque characteristics are dependent upon the relationship between flux-linkage and rotor position as a function of current. The developed torque is proportional to the square of the current and the slope of inductance. Fig. 9 shows the inductance profiles for torque winding and radial force winding with various rotor positions and currents,

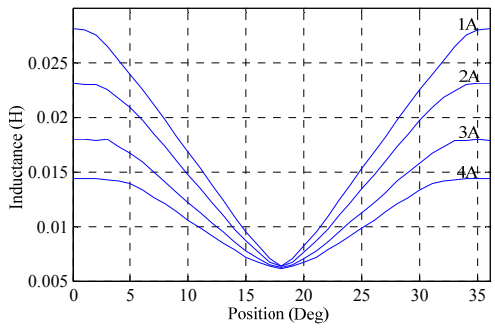

(a) Torque winding

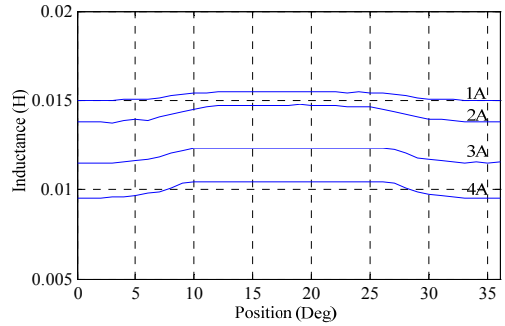

(b) Radial force winding

Fig. 9. Inductance profiles of the proposed structure.

respectively. Core saturation rises with increasing phase current, whereas the maximum inductances of the two types of windings decrease. Unlike torque winding, the inductance profile of radial force winding merely changes due to rotor position with the same phase current.

The set of generated torques for the two types of windings is shown in Fig. 10. The torque generated by radial force winding is small compared with that by torque winding.

Fig. 10 may have resulted from the very small variation in the inductance ratio of the radial force winding pole according to rotor position. Therefore, radial force control has almost no influence on torque control at an arbitrary rotor position. Decoupling control between torque and radial force can be realized naturally with the proposed BLSRM structure.

To explain the merits of the proposed structure, radial forces in conventional BLSRMs and the proposed structure are compared in Fig. 11.

Radial force in the proposed structure almost remains constant despite variations in rotor position. However, in conventional structures, radial force noticeably varies with rotor position. For higher radial force, the current in radial force winding in the conventional structure has to be increased.

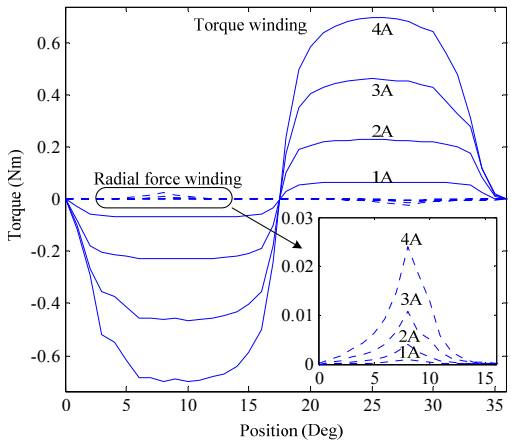

Fig. 10. Torque profiles of proposed structure..

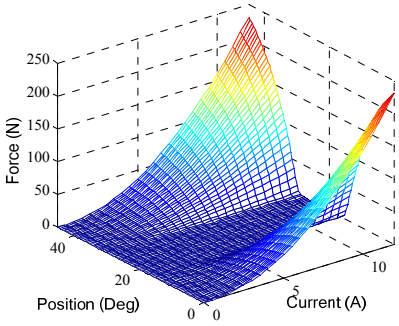

(a) Conventional structure

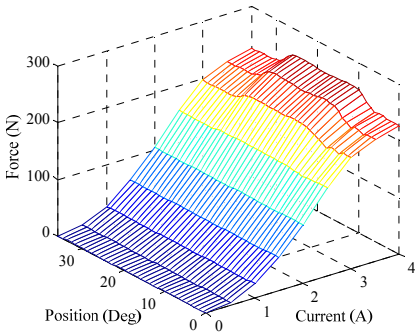

(b) Proposed structure

Fig. 11. Comparison of the radial force.

3.2 Eccentric Effect of the Rotor

Figs. 12 and 13 show the radial force generated by radial force winding P_{x4} under the center position, and at 33%, and 67% eccentric positions. As shown in both figures, the variation in radial force is more obvious. The force value in the y-direction also increased at the same rotor position due to rotor eccentricity. When the rotor is in the center position, the force value in x-direction F_x changes from positive to negative. However, when rotor undergoes eccentricity at x-direction, F_x also moves in the x-direction, but y-direction remains the same.

Fig. 13 shows the unbalanced magnetic pull force of torque winding A with different eccentricities.

According to Fig. 13, with increase in eccentricity, the values of an unbalanced magnetic pull force in two directions increase at the same rotor position. However, unbalanced magnetic pull forces in two directions are symmetric with respect to the angular bisector of the second quadrant, although with eccentricity in the x- or y-direction.

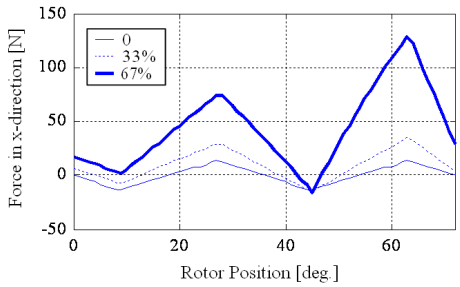

(a) Radial force in x-direction

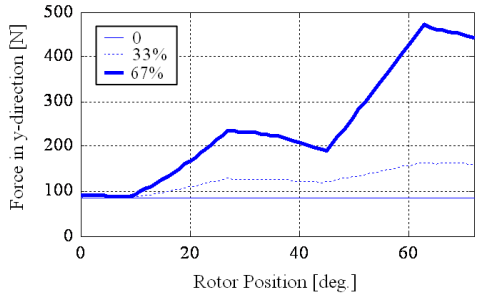

(b) Radial force in y-direction

Fig. 12. Radial force with eccentricities.

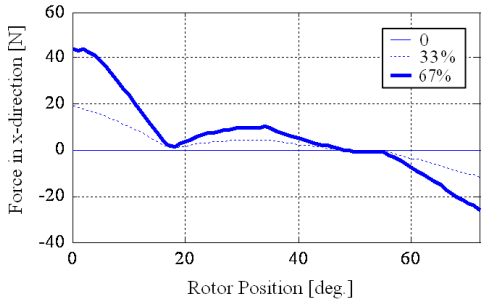

(a) Unbalanced magnetic pull force in x-direction

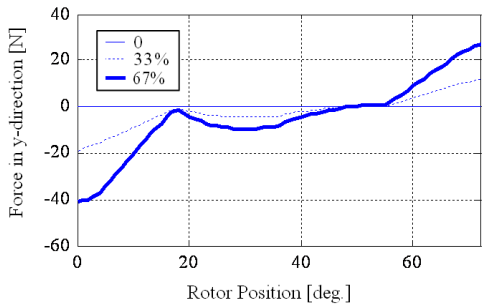

(b) Unbalanced magnetic pull force in y-direction

Fig. 13. Force with eccentricities.

Fig. 14 shows the torque profiles for radial force winding with different eccentricities. Eccentricity can considerably affect torque characteristics.

With increase in eccentricity, peak torque can also be increased. Since air-gap distribution changes with rotor rotation, the torque characteristic may lose its symmetry. The torque characteristic of each phase is not repeated identically at every circle. For example, the torque characteristic of winding A between 0 and 36° is different with the region between 36° and 72°.

Fig. 15 shows the torque characteristic of the radial force winding. The variation and peak value of torque generated by radial force winding from an eccentricity effect is much smaller than the one generated by torque winding. This may be due to the pole arc of radial force winding that is not less than one rotor pole pitch. Although air-gap distribution changes with rotor rotation, the slope of inductance with respect to rotor position is smaller than that of torque winding.

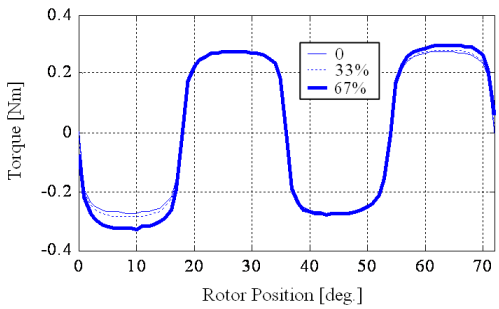

(a) Eccentricity in x-direction

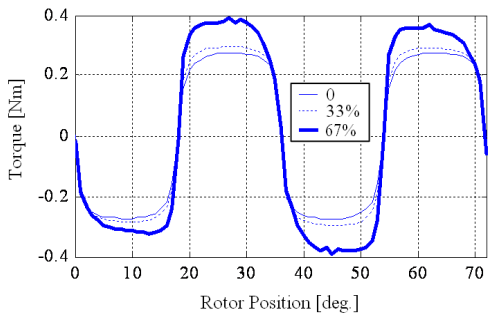

(b) Eccentricity in y-direction

Fig. 14. Torque characteristic of torque winding.

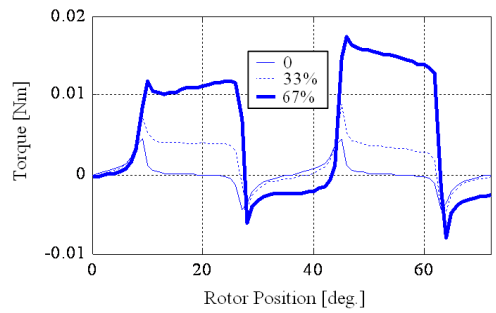

(a) Eccentricity in x-direction

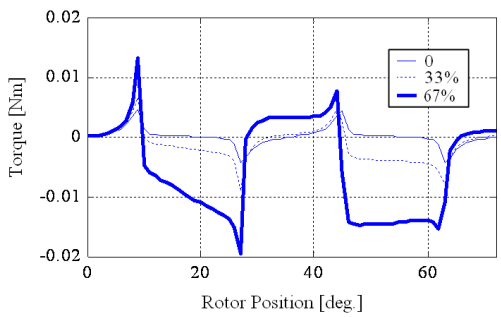

(b) Eccentricity in y-direction

Fig. 15. Torque characteristic of radial force winding.

4. Prototype Motor and Hardware Implementation

Fig. 16 shows a prototype of the proposed BLSRM. The stator and rotor are laminated with M19 steel sheets. The main mechanical parameters of the prototype's motor structure are shown in Table 2.

Asymmetric converters are used for torque and radial force control to drive the proposed motor. Due to their advantages like capability of independent control for each phase and three switching modes, asymmetric converters have been widely applied. Fig. 17 shows the operating modes and connection of radial force winding using an asymmetric converter. As shown in Fig. 17, there are two IGBTs and two freewheeling-diodes in each phase. In the proposed drive, two sets of asymmetric converters are

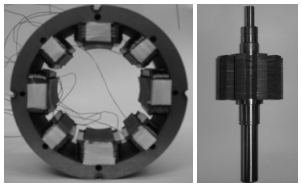

(a) Stator and Rotor

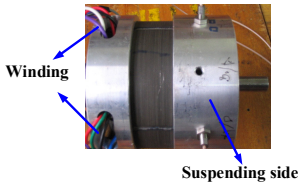

(b) Assembled prototype

Fig. 16. Prototype of proposed BLSRM.

Table 2. Main parameters of the prototype motor

Parameter	Value
Number of Stator Poles	8
Number of Rotor Poles	10
Pole arc of stator for torque (deg)	18
Pole arc of stator for radial force (deg)	36
Pole arc of rotor (deg)	18
Length of axial stack (mm)	40
Outer Diameter of Stator (mm)	112
Inner Diameter of Stator (mm)	62
Yoke Thickness of Stator (mm)	10
Length of Air Gap (mm)	0.3
Inner Diameter of Rotor (mm)	18
Yoke Thickness of Rotor (mm)	9.7

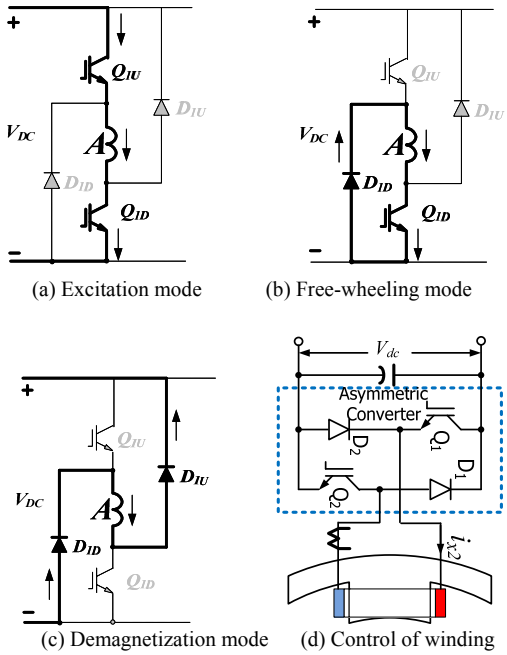

(a) Excitation mode (b) Free-wheeling mode

(c) Demagnetization mode (d) Control of winding

Fig. 17. Operating modes of asymmetrical converter.

adopted for four radial forces and two torque windings. Table 3 shows a comparison of results based on the number of power switches in some motor structures.

From Table 3, a motor drive system based on the proposed structure needs only 12 power switches. This value is lower than for conventional BLSRM drives. Thus, this system is cost-effective.

Table 3. Comparison of the number of power switches

BLSRM structures	Number of power switches		
	Torque winding	Radial force winding	Total
Differential winding (12/8 SRM)	2/phase	2/phase	18
Single winding (12/8 SRM)	2/phase		24
Single winding (8/6 SRM)	2/phase		16
Proposed Structure (8/10 SRM)	2/phase	2/phase	12

5. Experimental Results

Fig. 18 shows a comparison between FEM analysis and experimental measurements. Clearly, the measured inductances are well matched with FEM analysis. Inductance variation in the radial force pole is very small in relation to rotor position.

Fig. 19 shows the flux linkage characteristics for both windings. For torque winding, aligned and unaligned positions are considered with current variations.

For radial force winding, one rotor pole pitch is considered with currents from 1 to 3 A. The obtained experimental results are similar with those for the FEM results.

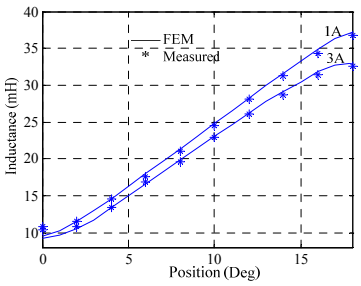

(a) Torque winding

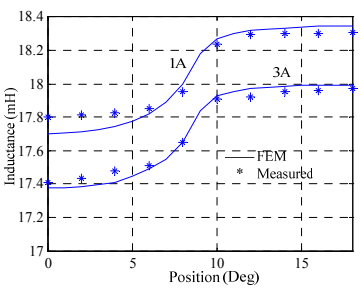

(b) Radial force winding

Fig. 18. Comparison of measured and FEM inductances.

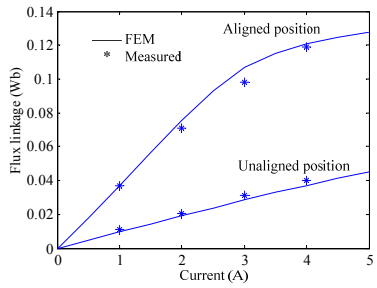

(a)Torque winding

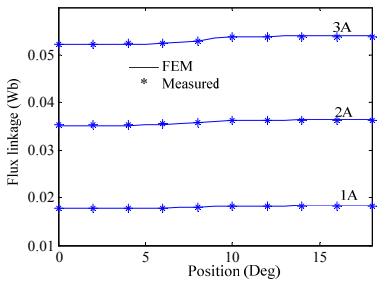

(b) Radial force winding

Fig. 19. Comparison of measured and FEM flux linkages.

Fig. 20 shows the control scheme of the proposed SRM. The eccentric displacements of the rotor in both directions have been measured by non-contact eddy current gap sensors. These two detected displacement signals can be used as feedback for radial position control.

PI-type controller is adopted to regulate motor speed. PWM duty ratio is obtained from the current controller, denoted as CCS in Fig. 20. By combining this with the current rotor position detected from the encoder, in-coming and off-going phases can be determined. Rotor radial position can be regulated by two independent close-loop air-gap displacement controllers, one for the x- and the other for the y-direction, respectively. These two PID controllers generate the desired radial force commands, F_x^* and F_y^*, to keep the rotor positioned at the center. The actual current

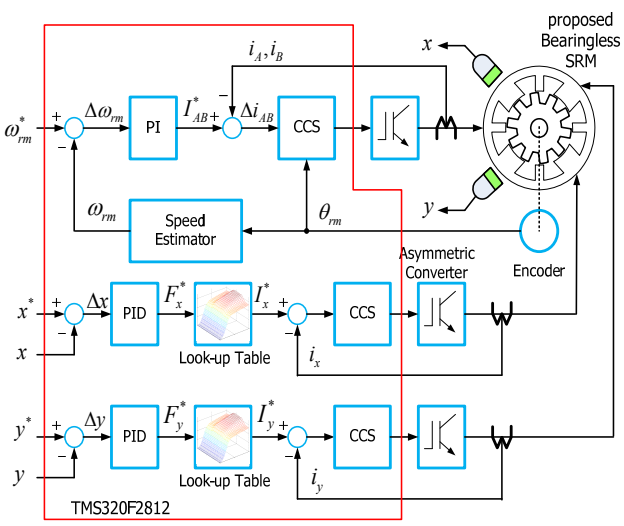

Fig. 20. Control scheme for the proposed BLSRM.

values of the selected radial force windings can be controlled by the hysteresis method by using these two current command signals. The above control algorithms are realized using TI TMS320F2812 DSP.

In the suspending force winding, total loss consists mainly of copper and core losses. As shown in Fig. 21, when radial force load is fixed, the current is almost 1A. As a result, total loss of the two suspending force windings is 4.2 W. Fig. 22 shows total efficiency at 1000 rpm; the fixed radial force load for various output torques is also shown.

Based on Fig. 21, in accordance with the losses of the suspending windings, the efficiency of the system is enhanced with increase in output power. This can be attributed to the fixed speed and radial force load. In effect, the losses of the suspending windings are almost constant. Consequently, the ratio of losses of suspending windings to output power is smaller with the increase in output power. To improve total efficiency in the driving system, the output power should be increased. This can be realized by modifying motor structure, such as by increasing the number of stator and rotor poles.

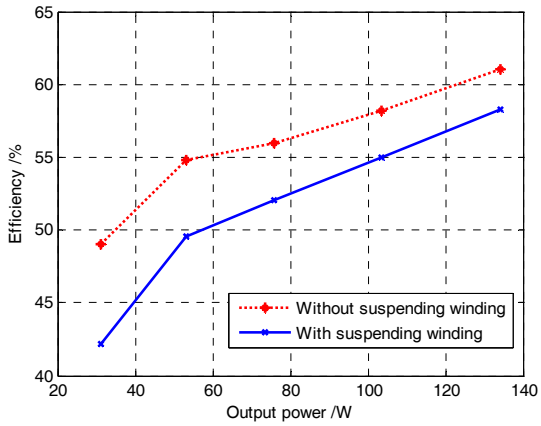

Fig. 21. Efficiency of the proposed BLSRM.

6. Conclusion

In this paper, the design and analysis of a novel 8/10 hybrid stator BLSRM are discussed. The radial force and basic design principle for the proposed structure are presented. Characteristics, such as inductance, torque, and radial force profiles of the two types of windings, are analyzed with the cases of non-eccentric and eccentric rotors. Some experimental results are also presented in order to verify the proposed structure. Both analysis and experimental results show that the proposed motor structure has a wider and larger radial force-generating region by a small excitation current. Torque control can be decoupled naturally from radial force control, which makes the proposed drive system simple and easy to use. Further research shall focus on high-speed drive with stable air gap regulation.

Acknowledgment

This work was supported by the National Research Foundation of Korea (NRF) grant funded by the Korea government (MEST) (Grant No. 2010-0014172).

References

[1] P. J. Lawrenson, J. M. Stephenson, T. T. Blenkinsop, J. Corda, and N. N. Fulton, "Variable-speed reluctance motors," *in Proc. IEEE, Pt. B*, Vol. 127, No. 4, July 1980, pp.253-265.

[2] N.R. Garrigan, W. L. Soong, C. M. Stephens, A. Storacc, and T. A. Lipo, "Radial force characteristics of a switched reluctance machine," in Proc. IEEE IAS Annu. Meeting, 1999, Vol.4, pp.2250-2258.

[3] I. Husain, A. Radun, and J. Nairus, "Unbalanced force calculation in switched reluctance machines," IEEE Trans, Magn., Vol.36, No.1, pp.330-338.

[4] M. Takemoto, A. Chiba, H. Akagi, and T. Fukao, "Radial Force and Torque of a Bearingless Switched Reluctance Motor Operating in a Region of Magnetic Saturation" in Conf. Record IEEE-IAS Annual Meeting, 2002, pp. 35-42.

[5] M. Takemoto, K. Shimada, A. Chiba, and T. Fukao, "A Design and Characteristics of Switched Reluctance Type Bearingless Motors", in Proc. 4th Int. Symp. Magnetic Suspension Technology, Vol. NASA/CP-1998-207654, May 1998, pp. 49-63.

[6] Li Chen, Wilfried Hofmann, "Analytically Computing Winding Currents to Generate Torque and Levitation Force of a New Bearingless Switched Reluctance Motor", in Proc.12th EPE-PEMC, Aug, 2006, pp. 1058-1063.

[7] Carlos R. Morrison. Bearingless Switched Reluctance Motor. U.S. Patent 6,727,618, 2004.

[8] A. V. Radum, "Design considerations for the switched reluctance motor," IEEE Trans. Ind. Applicat., Vol. 31, pp.1079-1087, Sep./Oct. 1995.

[9] M. N. Anwar, Iqbal Husain, and A. V. Radun, "A comprehensive design methodology for switched reluctance machines," IEEE Trans. IAS, Vol. 37, pp. 1684-1692, Nov/Dec, 2001.

Dong-Hee Lee was born on Nov. 11, 1970 and received his B.S, M.S., and Ph. D degrees in Electrical Engineering from Pusan National University, Pusan, Korea in 1996, 1998, and 2001, respectively. He worked as a Senior Researcher of Servo R&D Team at OTIS-LG, from 2002 to 2005. He has been with Kyungsung University, Pusan, Korea as an Assistant professor in the Department of Mechatronics Engineering since 2005. His major research field is Power Electronics and motor control system.

Jin-Woo Ahn was born in Busan, Korea in 1958. He received his B.S., M.S., and Ph.D. in Electrical Engineering from Pusan National University, Pusan, Korea in 1984, 1986, and 1992, respectively.

He has been with Kyungsung University, Busan, Korea. as a professor in the Department of Mechatronics Engineering since 1992. He was a visiting researcher in the Speed Lab at Glasgow University, U.K., a visiting professor in the Dept. of ECE and WEMPEC at the University of Wisconsin-Madison, USA, and a visiting professor in the Dept. of ECE at Virginia Tech. from July 2006-June 2007. He became director of the Advance Electric Machinery and Power Electronics Center. He also became director of the Smart Mechatronics Advanced Research and Training Center since Aug. 2008 and the Senior Easy Life Regional Innovation System since July 2008, which are authorized by the Ministry of Knowledge Economy, Korea. He is the author of five books including SRM, the author of more than 100 papers, and has more than 13 patents. His current research interests are advanced motor drive systems and electric vehicle drives.

Dr. Ahn received several awards including the Best Paper Award from the Korean Institute of Electrical Engineers in 2002, Korean Federation of Science and Technology Society in 2003, and Korean Institute of Power Electronics in 2007, and Park Min-Ho Academic Achievement Award from the Korean Institute of Electrical Engineers in 2009, respectively. He is a senior member of the Korean Institute of Electrical Engineers, a member of the Korean Institute of Power Electronics, and a senior member of the IEEE.